Submitted to Phys. Med. Bio., November, 2000

Experimental Apparatus to Measure the Effects of Strong Longitudinal Magnetic Fields on Photon and Electron Radiotherapy Beams

Dale W. Litzenberg, Benedick A. Fraass, Daniel L. McShan
University of Michigan, Department of Radiation Oncology, Ann Arbor, MI 48109-0010

Thomas W. O'Donnell, Donald A. Roberts, Fredrick D. Becchetti
University of Michigan, Department of Physics, Ann Arbor, MI 48109-1120

Alex F. Bielajew
University of Michigan, Department of Nuclear Engineering and Radiological Sciences, Ann Arbor, MI 48109-2104

Jean M. Moran
University of Michigan, Department of Radiation Oncology, Ann Arbor, MI 48109-0010

E-mail: litzen@umich.edu

Abstract. Monte Carlo studies have proposed that strong longitudinal magnetic fields can reduce the lateral scattering of primary and secondary electrons to reduce penumbra. In this paper we describe an experimental apparatus using a 3.5 Tesla superconducting solenoidal magnet to investigate the effect of longitudinal magnetic fields on electron and photon radiotherapy beams. The effects were studied using film in air and in phantoms which fit in the magnet bore.

The magnetic field focussed and collimated the electron beams. The converging, non-uniform field confined the beam and caused it to converge with increasing depth in the phantom. Due to the field's collecting and focussing effect, the beam flux density increased leading to increased dose deposition near the magnetic axis, especially near the surface of the phantom. Though the technique introduces some challenges associated with electron focussing, it shows promise for confining and focussing primary and secondary electrons during treatment.

The dose delivered by electron and photon radiotherapy beams results from the displacement and transport of electrons. These electrons are either primary particles, in the case of electron beams, or secondary particles set in motion by primary photon beams mostly through Compton recoil interactions. Electrons, once set in motion, scatter and lose energy randomly due to elastic and inelastic collisions. This increases the penumbra along beam edges, and can cause electronic disequilibrium in the vicinity of heterogeneities. In the case of electron beams, the resulting penumbra is quite broad making electrons quite difficult to use for conformal therapy. It has long been known that the application of a strong magnetic field to the scattering material, parallel to the beam axis, should reduce the lateral scattering of electrons (Bostick, 1950). Monte Carlo simulations (Bielajew, 1993) have demonstrated that very strong uniform longitudinal magnetic fields (20 Tesla) could reduce the lateral spread of 10 and 20 MeV electrons from many centimeters to a few millimeters. More moderate field strengths (3 to 6 Tesla) would also significantly reduce the penumbra. Bielajew's simulations have also shown that uniform longitudinal fields should not disturb local electron equilibrium. Additional

Monte Carlo studies by Ramahi et al. (Ramahi, 2000) have calculated that longitudinal magnetic fields could potentially reduce lateral electron scatter in photon-beam radiotherapy for water-air-water heterogeneities. In that study, electronic equilibrium was improved in planar water-air-water slab geometries exposed to a 6 MV photon beam by applying a longitudinal 0.5 Tesla uniform field to the phantom.

The effect of strong longitudinal magnetic fields on photon and electron beams had not been verified experimentally until now. We designed a setup to study the predicted behavior using 0.5 and 3 Tesla longitudinal magnetic fields. This paper describes the experimental setup and shows the general effect of a 3 Tesla magnetic field on 10 MeV and 20 MeV electron beams. More detailed results and analysis will be presented in future reports.

The experiment was conducted using the high-energy (G50) gantry of a two-gantry racetrack microtron accelerator (MM50 Scanditronix, Uppsala, Sweden). The photon and electron beams of the high-energy gantry have been previously described. (Karlsson, 1992, 1993) The basic characteristics of the electron beams are as follows. Electrons are accelerated in 5 MeV increments with clinical beam energies ranging from 10 to 50 MeV. The collimator head is filled with helium to reduce scatter. The beam is magnetically scanned in a hexagonal pattern such that a uniform field results. A small scattering foil is used to increase the FWHM of the beams in clinical mode, for energies greater than 10 MeV. Measurements for these experiments were made with the clinical 10 and 20 MeV electron beams with the scattering foil. Elemental pencil beams can also be produced without a scattering foil. Measurements were made at 50 MeV, with the scattering foil removed, to produce pencil beam of electrons coincident with the central axis.

Photon beams with energies of 10 and 25 MV are also available on the G50 gantry. Uniform photon beams were produced by magnetically scanning the electron beam on a thin, high-Z target in a concentric circular pattern such that a uniform field is produced. A purging magnet is used to remove collimator-generated electrons from the field.

A superconducting solenoidal magnet, with a 20 cm diameter, room-temperature bore, was used to produce a longitudinal field with a maximum strength of 3 Tesla near the center of the magnet. The properties of this magnet are shown in Table 1 (Stern, 1987). Simulation results not reported herein confirm that this field strength would be sufficient to observe a significant reduction in lateral electron scatter. A schematic of the experimental setup is shown in Figure 1. The magnet was supported by, and fastened to, an aluminum frame, which was bolted to the treatment room floor. The experiment was designed such that the photon and electron beams would enter the magnet along the magnetic axis. The orientation and position of the magnet's cryostat, relative to the electron beam, was determined by iteratively acquiring radiographs of pencil-beam electrons on films registered to the front and back of the cryostat using XV film (Kodak, Ready Pack). This axis was parallel to the horizontal beam axis within 0.5 degrees and aligned within one centimeter at the front of the magnet. The position of the coils within the cryostat are not precisely known, but the field map (previously measured with a Hall probe) indicates that the magnetic axis closely coincides with the air-bore axis, but is

slightly offset from the center of the cryostat along the axis. The peak field strength along the axis occurs 22.4 cm from the end of the cryostat closest to the gantry.

Table 1: Specifications of the superconducting solenoidal magnet.

magnet coil length	35.8 cm
magnet coil inner diameter	22 cm
magnet coil outer diameter	26 cm
Inductance	~ 12.5 Henry
Stored energy (@ 3.5 Tesla)	~ 100 KJ
Maximum central field	3.5 Tesla @ 125 amps
Power supply	IGC-180 M (+/- 4 V, 180 amps)
Ramp time (0 to 3.5 Tesla)	25 minutes
Decay rate (persistent mode)	<= 10^(-4) / hour
Cryostat length	47 cm
Cryostat bore diameter	20 cm
LHe Cryostat capacity	10 liters
LHe to cool down	50 – 70 liters
LHe to refill	15 liters
Power leads	LHe vapor cooled, non-retractable
Cryostat shielding	vacuum inner shield, LN outer shield
Hold time (persistent mode)	20 hour

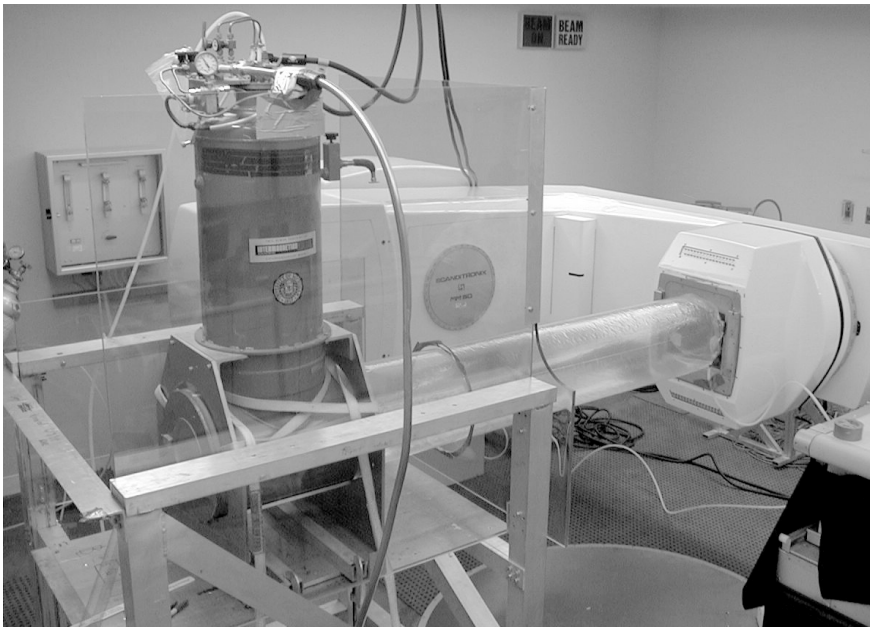

Figure 1: Photograph of the experimental setup. The G50 gantry is shown at the right with the solenoid magnet on the left. The beam was transported roughly 1.5 meters from the gantry exit window to the front face of the cryostat through a thin-walled, helium-filled, plastic tube to minimize scatter. Cylindrical phantoms were placed in the bore of the magnet to make film measurements.

The magnet was placed as far as possible from the gantry to reduce effects of the magnetic field on the beam optics of the accelerator. The magnetic center was 249 +/- 1 cm from the vacuum exit window. A fit to measured data (Figure 2) shows the field strength at the exit window of the treatment head, on the magnetic axis, was approximately 4×10^{-4} Tesla for an unperturbed field. The primary component of the

field is, in principal, parallel to the electron beam and only deflects those electrons that have a velocity component not directed along the magnetic axis. These particles with off-axis velocities arise from divergence and scattering of the beam.

To prevent degradation of the beam before reaching the magnet bore, a helium-filled plastic bag (29 cm diameter) was used to transport the beam from the treatment head to the front face of the magnet. The electrons were collimated using a 5 cm thick aluminum aperture with a 5 cm inner diameter opening. This collimator was placed in air, inside the magnet bore, with its front surface flush with the magnet cryostat's front face and the aperture centered on the axis of the magnet's air-bore. Cylindrical phantoms were designed and built to fit inside the magnet's 20 cm diameter bore.

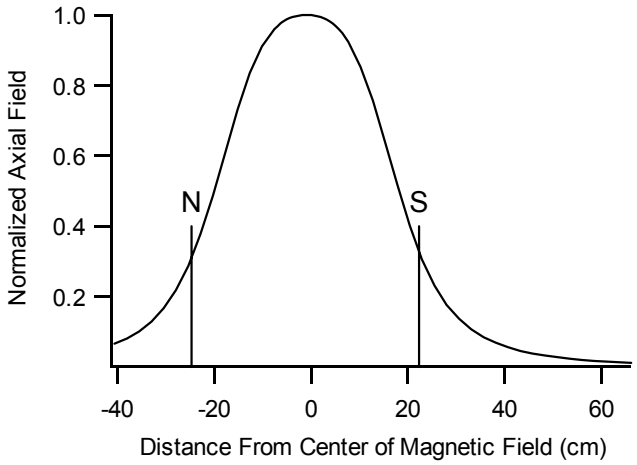

Figure 2: Measured field strength along the magnetic axis, normalized to the maximum field strength. The lines labeled N and S show where the north and south ends of the cryostat are relative to the peak value of the magnetic field.

To observe the effect of the magnetic field on a 10 MeV electron beam, films were placed at the gantry head exit window and on the front and back face of the magnet's cryostat. These distances corresponded to 70 cm, 226 cm and 273 cm from the source, respectively. Figure 3 shows the uniformity of the field exiting the treatment head when no magnetic field was present.

Figure 4 shows the digitized films for the 10 MeV beam when a magnetic field with a peak strength of 3 Tesla was present. It can be seen in Figure 4a that the beam exiting the collimator is no longer uniform over the field. This beam approaches the magnet on-axis, through the magnet's fringe field, in a helium atmosphere. This non-uniform beam has collapsed to a circle with significant radial structure at the front face of the magnet where the axial field strength is approximately 0.9 T (Figure 4b). The beam then enters air and passes through a 5 cm diameter, 5 cm thick aluminum collimator before traversing the bore of the magnet. The collimator has removed the outer portion of the beam and the beam has been focused to a FWHM of 1.54 cm as it exits the solenoid (Figure 4c).

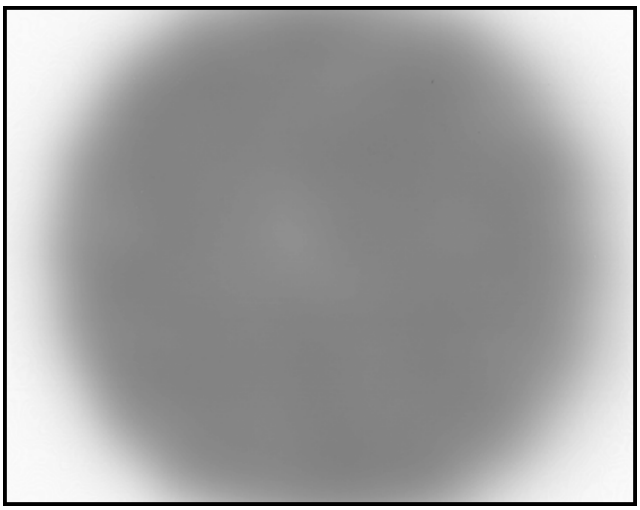

Figure 3: Digitized film showing a uniform 10 MeV electron beam exiting the gantry head when no magnetic field is present in the solenoid.

Figure 4a shows that the magnetic field has interfered with the beam transport optics at this energy. This indicates that the steel in the gantry has acted as a partial magnetic yoke, warping the solenoidal field to some degree. Instead of producing a uniform field as expected from the uniform scan pattern, most of the dose is in a semi-circular pattern, with the chord vertical. As the beam approaches the magnet each electron is subject to the force given by equation:

$$\mathbf{F} = q\mathbf{v} \times \mathbf{B} \tag{1}$$

where q is the charge on the electron, **B** is the magnetic field, and **v** is the electrons velocity, which is only slightly varying in the helium atmosphere. The converging fringe field collects and focuses the beam into the magnet. Electrons whose velocities are directed mainly along the magnetic axis experience relatively little force and are focused into the magnet along the converging magnetic field lines forming the dark central peak. Electrons scattered through larger angles that would normally be removed by electron cone collimators are also focused into the magnet and form the continuum of dose outside the central peak. The backscatter from the edge of the 5 cm inner diameter collimator is also seen. The beam is then collimated to 5 cm diameter as it enters the cryostat leaving primarily the central peak, as seen at the exit of the cryostat on the films. The beam has traveled through 47 cm of air in the bore of the magnet at this position, which has increased the FWHM diameter of the central peak due to scattering.

This effect on the beam trajectory, before reaching the phantom, has been demonstrated by Monte Carlo simulation (Weinhous, 1985). Simulations have not been carried out that include warping of the solenoidal field due a ferrous gantry. However, due to the symmetry of the field shown in Figure 4b, this perturbation of the field does not appear to significantly affect the trajectory of the electrons before reaching the phantom.

The effect of the 3 Tesla magnetic field on the beam trajectory and the dose profiles was significant for all electron beam energies. An example distribution, measured with film, is shown in Figure 5 for 20 MeV electrons with 0 T and 3 Telsa magnetic fields. Figure 5a shows the typical distribution expected for electrons. In this case, no magnetic field was present and the beam was collimated to 5 cm in diameter. Figure 5b shows the distribution produced by the beam when a 3 Tesla field is present under otherwise identical conditions. Notice that the field has perturbed the distribution in a number of ways. Firstly, the width of the beam at the surface of the phantom is smaller (3.3 cm FWHM compared to 4.9 cm). Secondly, the distribution is pinched inwards at a depth (1.8 cm FWHM compared to 5 cm at a depth of 3 cm). The typical bowing out of the distribution toward the end of the electron range (Figure 5a) is not seen with the magnetic field present (Figure 5b). This effect was also seen for the other electron beam energies. (Note that the grayscale windowing and leveling on Figures 5a and 5b are not the same to highlight the features on the individual films.)

Although both beams were programmed for the same number of monitor units, the film exposed with the magnetic field present had a much higher maximum optical density. This is the result of the converging, non-uniform magnetic field collecting and focussing electrons onto the magnetic axis. Thus many of the electrons that normally would have been scattered out of the beam or removed by an applicator in the absence of a magnetic field, now enter the phantom. In addition, the converging magnetic field has reduced the effective aperture causing the electron flux density to greatly increase. This effect indicates that dosimetry measurements conducted with no magnetic field would not be valid in the presence of a strong solenoidal field as

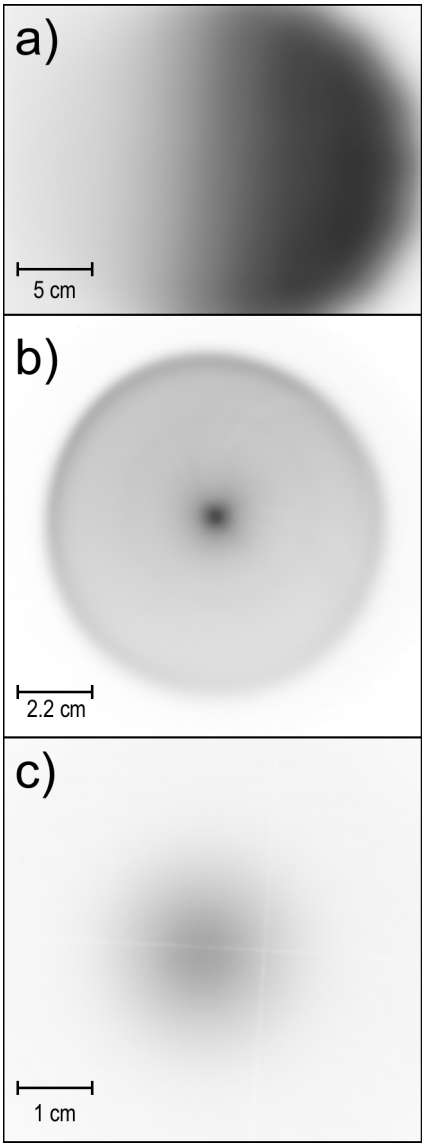

Figure 4: Digitized film showing a lateral profile of a 10 MeV electron beam when the peak magnetic field in the solenoid is 3 Tesla. Figure 4 a) shows that the beam exiting the gantry head is not uniform, b) shows the beam at the front surface of the magnet's cryostat and c) shows the beam at the back surface of the cryostat.

previously believed from simulation results which approximated the field as uniform in the phantom (Bielajew, 1993). However, an aperture placed between the exit window of the gantry and the front of the magnet could be used to reduce the angular acceptance of the magnet reducing the observed focussing effects.

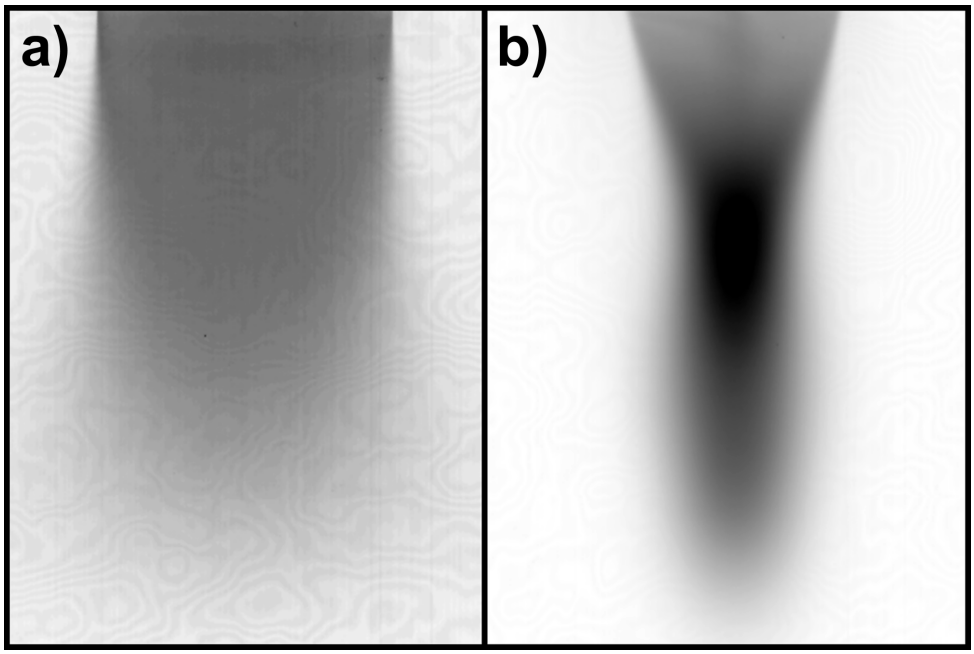

Figure 5: Digitized film showing the depth dose characteristics of a 20 MeV electron beam after passing through the 5 cm collimator in the magnet's bore. Figure 5 a) shows the beam when no magnetic field is present b) shows the beam when the peak magnetic field in the solenoid is 3 Tesla.

There is also a rather large field-strength gradient over the length of the distribution. The front of the phantom is located about 17 cm from the magnetic center, where the field strength is approximately 1.7 Tesla (Figure 2). The field strength 10 cm into the phantom, or 7 cm from the magnetic center, is approximately 2.8 Tesla. Therefore, as the electrons lose energy and scatter through larger angles they experience a much stronger force that confines and focuses the beam. While it is possible to modify the field gradients near the magnet with trim coils to tailor this focusing effect, the beam would still have to approach the magnet on axis through a dipole field and therefore experience a converging field with a strong gradient.

In the same way that electron beams may be manipulated with longitudinal magnetic fields, so may the electrons scattered by photon beams. Using the same setup as described above for electron beams, the effect of a longitudinal magnetic field on the characteristics of a 10 MV photon beam were also observed. Digitized films shown in Figure 6 illustrate the depth dose characteristics of this beam.

Figure 6a shows the beam when no magnetic field is present. The beam has passed through the 5 cm thick aluminum collimator. When a magnetic field is applied,

electrons are focused near the surface of the phantom. The focusing effect is larger for the 3 Tesla beam (Figure 6c) than for the 0.5 Tesla beam (Figure 6b).

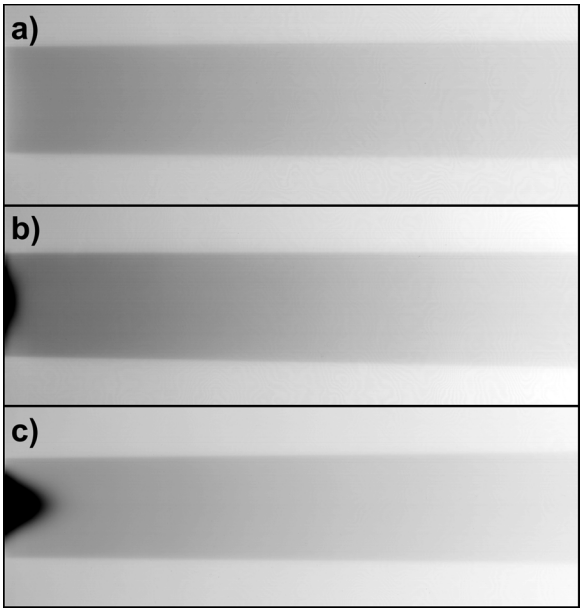

Figure 6: Digitized film showing the depth dose characteristics of a 10 MV photon beam after passing through the 5 cm Aluminum collimator in the magnet's bore. Figure 6 a) shows the beam when no magnetic field is present b) shows the beam when the peak magnetic field in the solenoid is 0.5 Tesla and c) shows the beam when the peak magnetic field in the solenoid is 3.0 Tesla.

In summary, we describe an experimental setup, using a superconducting solenoidal magnet, to investigate the effect of strong longitudinal magnetic fields on clinical electron and photon beams. The effect of the magnetic field on the beam trajectory was larger than anticipated and displayed a magnetic focussing and collimating effect on the beam. These effects were measured with film placed longitudinally or laterally in homogenous cylindrical phantoms. The phantoms were positioned near one end of the magnetic bore where the electrons experienced a strong field-strength gradient over their stopping range. In addition, the converging, non-uniform field not only confined the beam but also caused it to converge with increasing depth into the phantom. Due to the collecting and focussing effect of the solenoidal field the beam flux density increased, leading to increases in the observed dose deposition along the magnetic axis, especially near the surface of the phantom. There is no evidence of dose enhancement at the end of the electron's range. Although the technique introduces some difficulties with focussing scattered electrons into the field, it shows promise for confining and focussing primary and secondary electrons during treatment.

References

Bielajew A F, The effect of strong longitudinal magnetic fields on dose deposition from electron and photon beams, Med. Phys. 20 (1930) 1171-1179.

Bostick W H, Possible Techniques in Direct-Electron Beam Tumor Therapy, Phys. Rev. 77 (1950) 564-565.

Chu J C H, Reiffel L, Naqvi S, Li X A, Ye S-J, Saxena A, The use of magnetic fields to improve photon dose distributions for radiation therapy – a possible approach to "poor man's proton" beam properties, World Congress 2000 Proceedings. pp. 1-5

Ramahi S W, Naqvi S A, Chu, J, Achieving a smaller penumbra region for better planning in conformal radiotherapy by using a longitudinal magnetic field, World Congress 2000 Proceedings. pp. 1-5.

Stern R L, Becchetti F D, Casey T, Janecke J W, Lister P M, Liu W Z, Kovar D G, Janssens R V F, Vineyard M F, Phillips W R, Kolata J J, Tests of a large air-core superconducting solenoid as a nuclear-reaction-product spectrometer, Review of Scientific Instruments. 58(9); Sept. 1987; p.1682-93.

Weinhous M S, Nath R, Schultz R J, Enhancement of electron beam dose distributions by longitudinal magnetic fields: Monte Carlo simulations and magnet system optimization, Med. Phys., 15(5), 598-603, 1985.